Cement & Concrete Composites 44 (2013) 58–68

Contents lists available at SciVerse ScienceDirect

Cement & Concrete Composites

journal homepage: www.elsevier.com/locate/cemconcomp

An electrical impedance investigation into the chloride ion transport resistance of alkali silicate powder activated slag concretes

Deepak Ravikumar [a], Narayanan Neithalath [b,*]

[a] Solidia Technologies, Piscataway, NJ, United States
[b] School of Sustainable Engineering and the Built Environment, Arizona State University, Tempe, AZ 85287, United States

ARTICLE INFO

Article history:
Received 14 October 2012
Received in revised form 24 May 2013
Accepted 7 June 2013
Available online 14 June 2013

Keywords:
Alkali activated slag
Powder activator
Rapid chloride permeability
Non-steady state migration
Electrical impedance
Pore structure
Circuit models

ABSTRACT

The chloride transport resistance of alkali silicate powder activated slag concretes is evaluated. Two different Na_2O-to-source material ratios (n) and two SiO_2-to-Na_2O ratios of the activator (M_s) are used on concretes proportioned using two slag contents (300 kg/m^3 and 400 kg/m^3). Rapid chloride permeability (RCP) and non-steady state migration (NSSM) tests are used to evaluate the chloride transport behavior. Alkali silicate powder activated concretes demonstrate comparable or better chloride transport resistance than OPC concretes when evaluated using RCP and NSSM tests. The relationships between the activator parameter, $n{\cdot}M_s$, and the critical pore sizes (d_c) or the RCP and NSSM values demonstrate similar trends showing the influence of d_c in determining the ionic transport response. Electrical impedance spectroscopy (EIS) is used to relate the material response before and after the transport tests, and equivalent circuit models are used to extract the parameters that relate to the pore structure. EIS coupled with circuit modeling clearly brings out the differences between the RCP and NSSM test on their influences in the microstructure of alkali activated slag concretes.

1. Introduction

The need to reduce the consumption of portland cement because of its adverse environmental and energy-related impacts necessitates measures to develop alternate binding materials for concrete production. This has resulted in a variety of methodologies that either minimize or eliminate the use of ordinary portland cement (OPC) in concretes. The use of cement replacement materials such as fly ash and ground granulated blast furnace slag in high volumes in portland cement concrete has been established, as is the use of binders that do not contain any portland cement [1–3]. The latter category of binders is typically produced by activation of waste/by-product materials such as fly ash or slag by alkaline hydroxides or silicates.

Alkali activation of slag has been a subject of several reported studies [4–9]. The activating agent used typically is a sodium silicate-based solution ($Na_2SiO_3{\cdot}xH_2O$ + NaOH). It is well known that alkali activation of slag produces C–S–H gel as the main reaction product. The influence of several parameters relating to the source material and the activator that can potentially influence the reaction kinetics as well as the mechanical and durability properties of the final product has been reported [1,10–15]. A majority of the studies on alkali activated slags have been carried out using waterglass solution as the activator. This presents issues with handling because of the caustic nature of the alkalis. Hence, in this study, powder sodium silicate and sodium hydroxide are used as activating agents. This is also expected to help in the development of blended binder-activator systems which can be handled easily, and will develop its properties just by the addition of water. While the strength of such binder systems is generally lower than those activated by waterglass solutions, by proper proportioning procedures, compressive strengths in the range of 30–35 MPa can be achieved [16], which is sufficient for most of the common concrete applications. Detailed studies on the reaction kinetics and product formation in alkali silicate powder activated systems have been reported recently by the authors [16,17].

The pore structure of alkali activated slag concretes have been studied [18,19] and it is reported that these concretes have beneficial pore structure features when compared to OPC concretes. However, the use of a highly alkaline activating agent results in a higher pore solution conductivity. A combination of these two factors influence the transport of ionic species such as chlorides through alkali activated slag concretes. This paper investigates the chloride ion transport in alkali silicate powder activated slag concretes using two common accelerated chloride transport tests – the rapid chloride permeability (RCP; conforming to ASTM C 1202) and non-steady state migration (NSSM; conforming to NT Build 492) tests. The influence of pore structure on chloride ion

* Corresponding author. Tel.: +1 480 965 6023; fax: +1 480 965 0557.
E-mail addresses: dravikumar@solidiatech.com (D. Ravikumar), Narayanan.Neithalath@asu.edu (N. Neithalath).

0958-9465/$ - see front matter © 2013 Elsevier Ltd. All rights reserved.
http://dx.doi.org/10.1016/j.cemconcomp.2013.06.002

transport is quantified, and the changes in pore structure as a result of these accelerated chloride transport tests are estimated through the use of electrical impedance spectroscopy and associated equivalent electrical circuit modeling.

2. Experimental program

2.1. Materials and mixture proportions

Type 100 ground granulated blast furnace slag conforming to ASTM C 989 was used as the binding material in this study. The chemical composition of slag is shown in Table 1. The particle size distribution of slag is such that 95% is finer than 35 μm and the d_{50} is ~10 μm. Combinations of anhydrous sodium silicate powder (>99% sodium silicate and < 1% crystalline silica) having a SiO_2-to-Na_2O ratio (or the modulus, M_s) of 1.95, and analytic reagent-grade sodium hydroxide (NaOH) beads are used as the activating agents in this study. The sodium silicate powder has a median particle size of 25 μm and a pH of 12.6 (for a 50% w/v slurry in water). NaOH addition facilitated changing the activator M_s to lower values in order to obtain 28-day compressive strengths in the range of 20–30 MPa. The M_s (mass-based) values thus chosen are 0.60 and 1.50, and the corresponding molar-based M_s values are 0.62 and 1.55. The n values (Na_2O-to-slag ratio) used are 0.05 and 0.15. An example of the activator quantity determination is provided below. If a mixture with an n value of 0.05 and a mass-based M_s of 1.5 is required, for every 1000 g of slag, 50 g of Na_2O and 75 g of SiO_2 is required. Since sodium silicate powder is the only source of silica from the activator, 75 g of SiO_2 can be obtained from 114 g of sodium silicate powder which has an M_s of 1.95. The sodium silicate powder would also provide 39 g of Na_2O. The remaining 11 g of Na_2O (50–39 g) is then obtained by the addition of NaOH.

Several activated slag concretes were proportioned as part of this study. Concretes containing two different slag contents (300 kg/m^3 and 400 kg/m^3) were proportioned and activated using powder sodium silicate and NaOH. The effective water-to-powder ratio for the mixtures was maintained at 0.40. The powder consists of the slag, powder sodium silicate and NaOH. River sand was used as the fine aggregate and pea gravel with a nominal maximum size of 9.5 mm was used as the coarse aggregate. The moisture absorption of the aggregates was accounted for in the mixture proportioning. The mixture proportions are shown in Table 2. The specimens made using these mixture proportions were used for compressive strength and chloride transport studies after specified durations of curing in a moist chamber. Activated mortar samples with a paste volume fraction of 50% were used for the compressive strength tests and paste specimens were proportioned for the microstructural tests using the same water-to-powder ratio as used for the concretes. All the paste, mortar, and concrete specimens were removed from the molds after 24 h and moist cured in a humidity chamber (>97%RH) until the time of testing.

2.2. Test methods

The experimental technqiues used include the methods for accelerated determination of chloride transport paramertes, electrical impedance spectroscopy (EIS) before and after the chloride transport tests, and pore structure determination using mercury intrusion porosimetry (MIP). In addition, compressive strength of mortar specimens determined in accordance with ASTM C 109, and Fourier Transform Infrared (FTIR) Spectroscopy were used to bring out the difference in the properties and reaction products when powder or liquid forms of sodium silictae were used as activators.

Table 1
Chemical composition of slag.

SiO_2	Al_2O_3	CaO	Fe_2O_3	MgO	Na_2O	K_2O	SO_3	LOI
36.0%	10.5%	39.8%	0.67%	7.93%	0.27%	0.80%	2.1%	3.0%

2.2.1. Chloride transport test methods

Rapid chloride permeability (RCP) test in accordance with ASTM C 1202 and non-steady state migration (NSSM) test in accordance with NT Build 492 were carried out on 50 mm thick discs cut from 200 mm long cylindrical concrete specimens. For the RCP test, the specimens were conditioned by vacuum saturation, and enclosed in a cell flanked by reservoirs that contain 0.3 N NaOH solution on one side and 3% NaCl solution on the other. A 60 V potential difference was applied between the electrodes placed on both faces of the specimen, for a duration of 6 h. The total charge passed (in coulombs) at the end of 6 h of testing is reported as the RCP value. For the NSSM test, the specimens were preconditioned by vacuum saturation with $Ca(OH)_2$ solution. The catholyte and anolyte solutions used were 2 N NaCl and 0.3 N NaOH respectively. An initial voltage of 30 V was applied, and initial current recorded. The applied voltage and test duration were chosen based on the initial current. The test duration was maintained at 24 h and the voltage at 30 V for all the cases. After the test duration, the specimens were axially split and sprayed with a 0.1 M silver nitrate solution. The depth of chloride penetration was measured based on the precipitation of white silver chloride. The non-steady state migration coefficient (D_{nssm}) in m^2/s is given as:

$$D_{nssm} = \frac{RT}{zFE}\frac{x_d - \alpha\sqrt{x_d}}{t} \quad (1)$$

$$\alpha = 2\sqrt{\frac{RT}{zFE}}erf^{-1}\left(1 - \frac{2c_d}{c_0}\right) \quad (2)$$

$E = (U-2)/L$, where U is the absolute voltage (V), L is the specimen thickness in m, z is the valence of the chloride ion, F is the Faraday constant, R is the molar gas constant, T is the average value of initial and final temperatures in K, x_d is the average value of the penetration depth in m, t is the test duration in seconds, c_d is the chloride concentration at which silver nitrate changes to silver chloride (0.07 N), and c_0 is the chloride concentration of the catholyte solution (2 N). The value of c_d chosen for this study is the one generally used for OPC concretes. However, the calculations for D_{nssm} were repeated with c_d values of 0.05 and 0.1, but this resulted in insignificant changes to the D_{nssm} value. Hence a c_d of 0.07 itself is used in this study. While the use of RCP test for alkali activated slag concretes have been reported [20,21], the use of NSSM test for these systems is not reported, and further studies are needed to ascertain if the values of the constants used for OPC systems can be applied to alkali activated concretes also. This assumes more significance given our understanding of the limitations of the RCP test. In this paper, the NSSM coefficients are used as relative indicators of the transport properties of different mixtures, and hence the methodology adopted is considered to be adequate.

2.2.2. Electrical impedance spectroscopy (EIS)

Electrical impedance spectroscopy (EIS) was employed on specimens before and after they were subjected to the RCP and NSSM tests. EIS measurements were conducted in this study using a Solartron 1260™ impedance/gain-phase analyzer that was interfaced with a personal computer for data acquisition. The test set up is shown in Fig. 1a. The frequency of the EIS measurements ranged from 10 Hz to 1 MHz using a 250 mV AC signal, with 10 measurements per decade. The effective specimen conductivity (σ_{eff}) was determined from the bulk resistance (R_b) obtained from EIS. A typical Nyquist plot, which relates the real and imaginary imped-

Table 2
Mixture proportions for low slag and high slag content mixtures.

Slag content	n	M_s	Slag (kg/m^3)	Sodium silicate	NaOH	Water	Coarse agg.	Fine agg.
Low	0.05	0.6	300	13.3	13.3	130.6	1079.3	719.5
Low	0.05	1.5	300	34.1	4.3	135.4	1057.3	704.9
Low	0.15	0.6	300	40.9	40.9	152.7	1000.7	667.1
Low	0.15	1.5	300	102.4	12.9	166.1	937.5	625.0
High	0.05	0.6	400	18.2	17.7	174.4	958.4	638.9
High	0.05	1.5	400	45.6	5.7	180.5	929.6	619.8
High	0.15	0.6	400	54.6	53.3	203.2	855.7	570.4
High	0.15	1.5	400	136.6	17.2	221.5	769.9	513.3

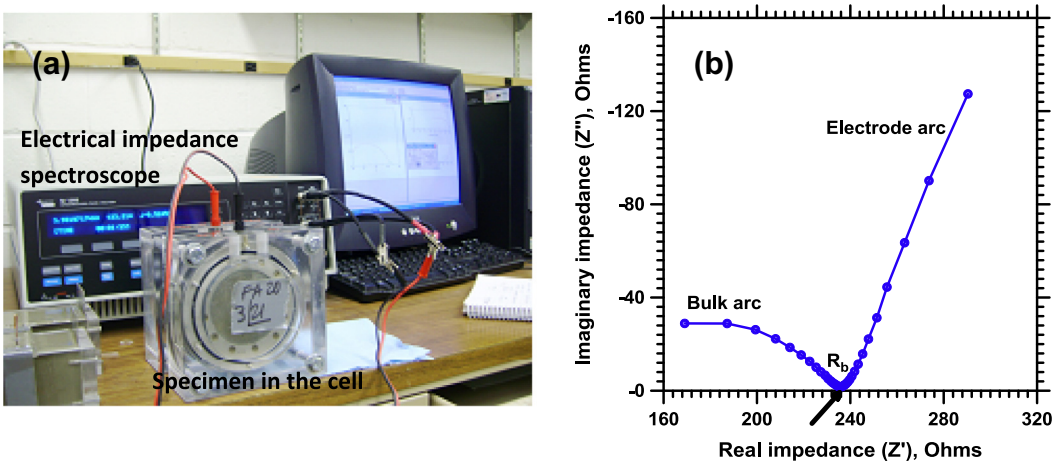

Fig. 1. (a) Electrical impedance spectroscopy test set up for the accelerated chloride transport test specimens, and (b) a typical Nyquist plot from EIS.

ance at different frequencies [22], is shown in Fig. 1b. The abscissa of the intersection of the bulk and electrode arcs in a Nyquist plot is the bulk resistance, from which the effective conductivity (σ_{eff}) can be calculated as:

$$\sigma_{eff} = \frac{L}{R_b A} \tag{3}$$

where L and A are the specimen length and cross-sectional area respectively. The Nyquist plot is used in conjunction with electrical circuit models for the microstructure to analyze the influence of chloride ingress on the microstructure as will be explained in a later section.

2.2.3. Pore structure using mercury intrusion porosimetry (MIP)

Mercury intrusion porosimetry (MIP) is a commonly used method to evaluate the pore structure in cementitious materials [23,24]. The applied pressure during the intrusion of mercury and the pore diameter are related through the Washburn equation [23]. MIP was carried out on small samples of oven-dried alkali activated pastes using a porosimeter that can generate a maximum pressure of 414 MPa and evaluate a minimum pore diameter of 0.003 μm. The test was performed in two steps – the low pressure step evacuates the gases, fills the sample holder with mercury, and carries out the test up to 345 kPa, and the high pressure step reaches pressures of up to 414 MPa. A contact angle of 130° and a surface tension of 0.485 N/m were used in the analysis.

3. Results and discussions

3.1. Activation of slag using powder and liquid sodium silicate: a comparison

Liquid sodium silicate (waterglass) of desired silica modulus (M_s) is commonly used as the activating agent to produce alkali activated binder systems. Powder sodium silicate is used in this study to activate slag because of its benefits in storage and handling. The mechanism of activation using powder sodium silicate and waterglass are different as has been recently elucidated by the authors using isothermal calorimetric and reaction product studies [16,17]. The difference in activation efficiency, in part, is due to the limits of silicate solubility in water at ambient temperatures, as has been demonstrated using FTIR spectra of the activator solution [16]. This results in different mechanical and transport properties for the liquid and powder activated concretes. Fig. 2a and b present a comparison of the compressive strength development of powder and liquid sodium silicate activated slag mortars, where the effectiveness of waterglass in activation can be distinctly noticed, the reasons for which have been elaborated earlier [16]. The differences in reaction products, demonstrated through a change in the wavenumber attributed to Si–O–Si stretching vibration are shown in Fig. 3. The wavenumbers for the waterglass activated pastes (around 975 cm^{-1}) confirm the presence of a conventional C–S–H gel whereas the presence of sodium silicate gel in addition to C–S–H [17] results in a higher wavenumber (1010–1025 cm^{-1}) for the powder sodium silicate activated pastes. The foregoing discussion provides a short summary of the contrasts in mechanical properties and reaction products of alkali silicate powder and liquid activation of slag, while [25] presents the contrasts in chloride ion transport responses of these systems. In this paper, the focus however is on the chloride ion transport properties of alkali silicate powder activated slag mixtures, and the use of electrical impedance to characterize the transport response and the microstructure.

3.2. Rapid chloride permeability (RCP) values of activated slag concretes and relationship with electrical response

Rapid chloride permeability test (RCPT), conforming to ASTM C 1202 is one of the common durability tests that is used as a quality

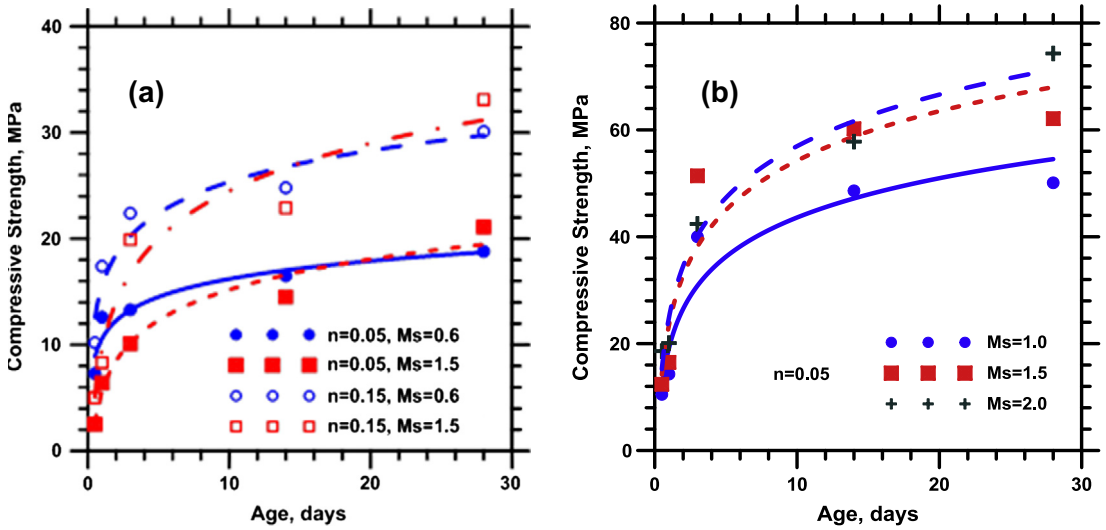

Fig. 2. Compressive strength development of: (a) alkali silicate powder activated slag mortars, and (b) waterglass activated slag mortars [16]. The standard deviations in compressive strength measurements range between 0.5 MPa at early ages to 5 MPa at later ages.

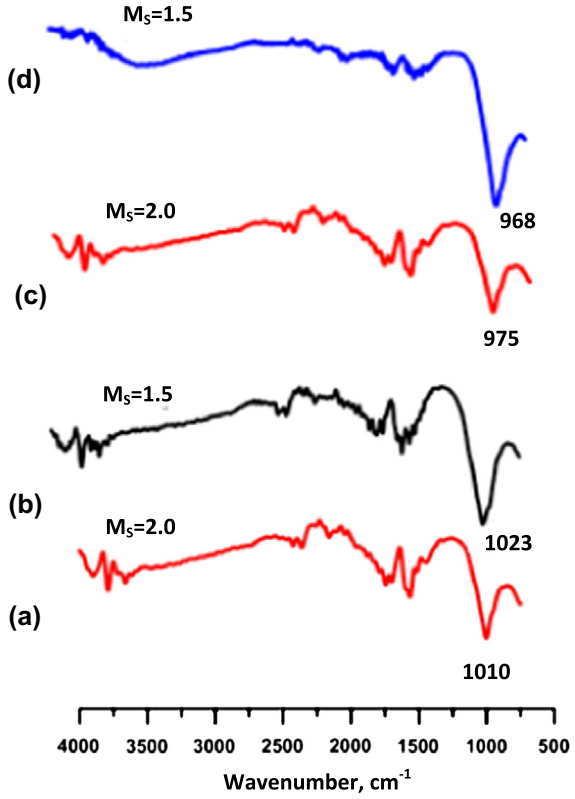

Fig. 3. FTIR spectra of alkali silicate powder (a and b) and waterglass (c and d) activated slag pastes [25].

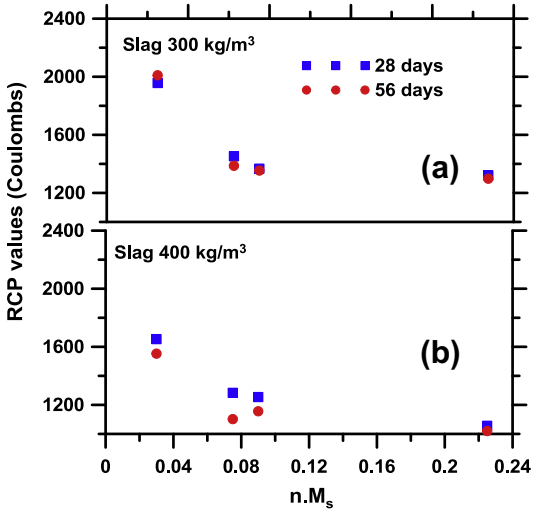

Fig. 4. Relationships the activator parameter ($n{\cdot}M_s$) and RCP values for activated concretes with slag contents of: (a) 300 kg/m^3, and (b) 400 kg/m^3.

control measure and acceptance criteria for OPC concretes. Fundamentally, RCP test measures the electrical resistance or conductivity of concretes. Conductivity of porous materials saturated with a conducting fluid (such as the pore solution in concretes) is greatly influenced by the conductivity of the saturating medium in addition to the pore structure parameters like the overall pore volume and its geometry. Thus this test does not adequately represent the pore structure characteristics of the material that are crucial in ionic transport. This aspect has been reported elsewhere in detail [26–28]. However, its ease of use and documented relationships with other performance characteristics of concrete has made this test widely accepted in practice.

3.2.1. RCP values of high and low slag content activated concretes

Fig. 4a and b show the RCP values of the low slag content (300 kg/m^3) and high slag content (400 kg/m^3) mixtures after 28 and 56 days of curing in moist environment. The RCP values are plotted as a function of the product of the Na_2O-to-slag ratio (n) and the SiO_2-to-Na_2O ratio (M_s) of the blended activator powder. This effectively is the ratio of the SiO_2 content of the activator to the total slag content. This parameter is significant because it has been shown that the later-age (14 days and beyond) compressive strengths of alkali silicate powder activated slag concretes is proportional to the SiO_2 content of the activator [17]. In general, it can be seen that the RCP values at all the ages considered, decrease with increase in $n{\cdot}M_s$ (or the silica content in the activator) initially, and beyond a $n{\cdot}M_s$ of about 0.10, there is essentially no change in the RCP values. This value of $n{\cdot}M_s$ can

be considered as a limiting value, beyond which any increase in silica content of the activator is not beneficial in changing any of the microstructural features that influence ionic transport as measured by the RCP test. Between 28 and 56 days, there is not much difference in RCP values, indicating that the later age reactions so common in OPC concretes with cement replacement materials are absent in the alkali silicate powder activated slag concretes.

The RCP values range between 2000 and 1300 Coulombs for the low slag content mixtures (28 and 56 days), and between 1700 and 1000 Coulombs for the high slag content mixtures. These values are lower than the RCP values of conventional concretes used in practice. The RCP values of solid sodium silicate activated slag concretes evaluated in this study are also lower than those of the alkali silicate liquid (waterglass) activated concretes reported recently by the authors [25] and are comparable to the RCP values of waterglass activated slag concretes reported in [20]. It needs to be noted that the alkalinity adopted for activation in both the above-referenced studies are different, resulting in the observed difference in RCP values. The differences in the RCP values as a function of slag content (300 kg/m^3 or 400 kg/m^3; see Table 1) can also be discerned from Fig. 4a and b. To put the obtained RCP values into perspective, a typical OPC concrete with a water-to-cement ratio (w/c) of 0.40 has a RCP value of about 3000 Coulombs after 56 days of curing, where as a mixture with 20% fly ash as cement replacement typically shows RCP values of about 2000 Coulombs after 56 days [27]. Concrete with 5% silica fume as cement replacement shows a RCP value of about 800 Coulombs after 56 days, but in this case the drastically reduced pore solution conductivity contributes to a part of the observed reduction in the RCP values [27]. Thus it can be noticed that the RCP values of alkali activated slag mixtures reported in this research are much lower than those of plain OPC concretes, but comparable to those of OPC concretes containing cement replacement materials such as silica fume or fly ash. This is notwithstanding a pore solution that is likely to be electrically more conductive due to the higher concentrations of Na^+ and OH^- ions [20]. The increased amounts of Na ions in the pore solution, especially in mixtures with high $n{\cdot}M_s$ values can be expected to lead to increased charge values because the Na^+ ions will counter-diffuse as the Cl^- ions are driven into the material through the application of electrical potential gradient. The fact that the RCP values remain low even under these circumstances can be considered as an indicator of the better chloride transport resistance of these concretes. The similarity of RCP values of the alkali silicate powder activated slag concretes to those of OPC concretes with a refined pore structure (due to the incorporation of fly ash or silica fume) point to the likely similarities in their pore structure features, which will be examined later in this paper.

3.2.2. Relationship between RCP values and electrical properties

Fig. 5a shows the relationship between the RCP values and the bulk resistance obtained from EIS. In general, there is a good relationship between the bulk resistance (or the conductivity extracted from bulk resistance using Eq. (3)) and the RCP values. However the relationship is not as good as the conductivity-RCP relationships generally observed for OPC concretes [27]. This could be attributed to a variety of reasons including the differences in pore structure (pore sizes and tortuosity) with changes in activator alkalinity, formation of sodium silicate gel in addition to C–S–H gel [17], and the presence of C–S–H with lower Ca/Si molar ratios where some of the Si is substituted by Al, and Na playing either a charge balancing role or being sorbed into the C–S–H structure. The conductivity of the solid phases in alkali activated solid systems could also greatly vary based on the activator alkalinity and the means through with the alkalis are incorporated into the reaction products. This changes the effective electrical properties of the system, in contrast to OPC systems where the solid phase can be reasonably estimated to have similar conductivities (of the order of 0.001–0.005 S/m) [29].

The changes occurring in the specimen as a result of chloride ingress during the RCP test can be ascertained by measuring the electrical conductivities of the specimens before and after the test. RCPT induces Joule heating in the specimens because of the higher voltage (60 V) applied for a 6 h duration [28]. Conductivity is dependent on the temperature, and hence the measurements after the RCP test were carried out after allowing the specimens to return to the ambient temperature. Fig. 5b shows the relationship between the effective conductivities before and after the RCP test for the alkali powder activated slag concretes proportioned using all the n and M_s values shown in Table 2. While a very good linear relationship is noticed between the conductivities before and after the test, the effective conductivities are higher by 14–19% after the RCP test. This can be plausibly attributed to: (i) the ingress of Cl^- ions into the concrete and the fact that there is no removal of other ions from the specimen during the RCPT duration, and (ii) microstructural damage induced by the higher applied voltage and the associated temperature increase.

3.3. Non-steady state migration (NSSM) coefficients of activated slag concretes and relationship with electrical response

The NSSM test avoids some of the drawbacks of the RCP test by using a lower applied potential (typically 30 V) and a longer test duration (24 h). The catholyte solution used is 10% NaCl, thereby ensuring that the catholyte concentration does not undergo large changes during the duration of the test.

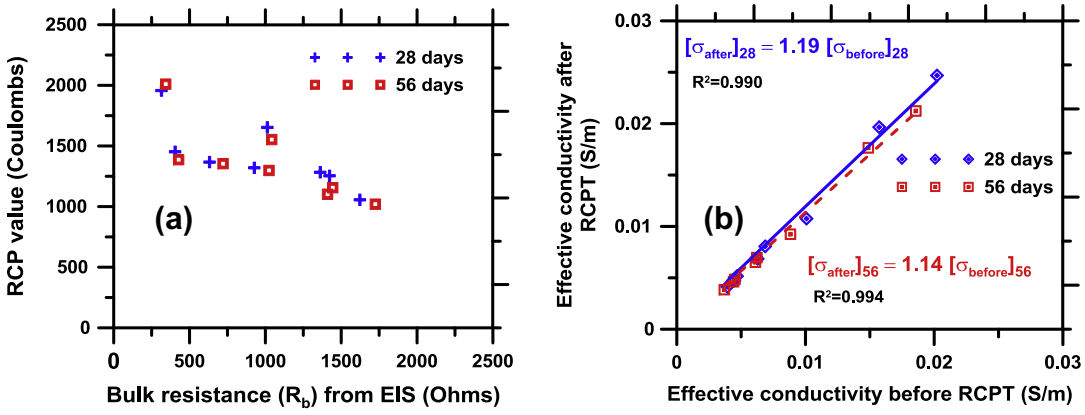

Fig. 5. Relationships between: (a) the bulk resistance (R_b) from EIS and the RCP values, and (b) effective specimen conductivities before and after the RCP test.

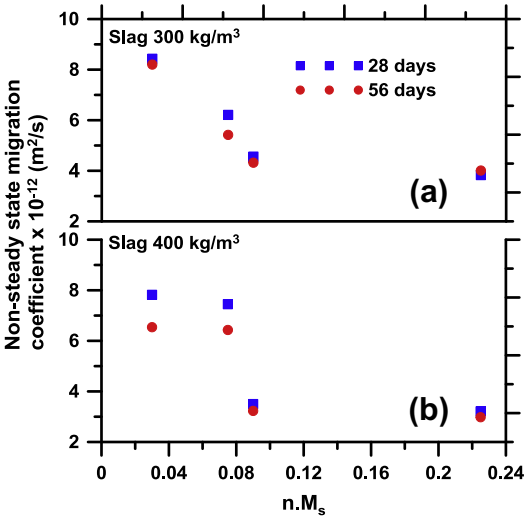

Fig. 6. Relationships the activator parameter ($n{\cdot}M_s$) and NSSM coefficients for activated concretes with slag contents of: (a) 300 kg/m^3, and (b) 400 kg/m^3.

3.3.1. NSSM coefficients of high and low slag content activated concretes

Fig. 6a and b depict the NSSM coefficients (D_{nssm}) of low slag and high slag content activated concretes cured for 28 or 56 days, as a function of the parameter $n{\cdot}M_s$. The general trend in the variation of D_{nssm} with $n{\cdot}M_s$ is similar to that of the RCP values, with a reduction in D_{nssm} with increasing $n{\cdot}M_s$ (or silica content of the activator) until the limiting $n{\cdot}M_s$ value of 0.10. Beyond that there is no appreciable change in D_{nssm}, the reasons for which were explained in a previous section. As observed from Fig. 6a and b, D_{nssm} of the alkali activated slag mixtures range between 3×10^{-12} m^2/s and 8×10^{-12} m^2/s. The higher slag content mixtures demonstrate lower D_{nssm} as expected. As a point of reference, a typical 56-day moist cured OPC concrete made using a w/c of 0.40 has a D_{nssm} of 8×10^{-12} m^2/s, while concretes where 20% or 5% of cement by mass is replaced with either fly ash or silica fume show D_{nssm} values of 5×10^{-12} m^2/s and 3×10^{-12} m^2/s respectively [27]. There are some similarities and contrasts that need to be brought out when the trends in the RCP and NSSM values of these mixtures are compared. They are summarized as follows: (i) the RCP values of alkali silicate powder activated slag concretes are lower than those of plain OPC concretes, (ii) the RCP values of activated slag concretes, irrespective of the $n{\cdot}M_s$ values, are comparable to those of OPC concretes modified with fly ash or silica fume, (iii) the NSSM coefficients of activated slag concretes of lower $n{\cdot}M_s$ values are comparable to those of plain OPC concretes, and (iv) the NSSM coefficients of activated slag concretes of higher $n{\cdot}M_s$ values are comparable to those of OPC concretes modified with fly ash or silica fume. Microstructural evaluation (overall pore volume and pore size distribution measurements) are carried out as described in a forthcoming section to shed more light into these observations.

3.3.2. Relationship between NSSM coefficients and electrical properties

When the NSSM coefficients are plotted as a function of the bulk resistances of the specimens before the test, the scatter is much more as observed in Fig. 7a, than that in the R_b–RCP relationship depicted in Fig. 5a. This is because RCP test is essentially a conductivity/resistivity test, and the factors influencing the RCP test are more or less the same as those influencing an electrical conductivity test. On the other hand, the NSSM coefficient (D_{nssm}) is obtained through considerations of ionic movement under an electric field. Under a potential difference, the ionic movement occurs through migration and diffusion. At applied voltages of more than 10–15 V, the diffusive component can be neglected, and the transport can be considered as solely through migration. The Nernst–Plank equation applies for the migration case, which is solved to obtain D_{nssm}. Thus it is not surprising that there is no direct correlation between the bulk resistance of the specimens and D_{nssm}. The effective electrical conductivity of the specimens before and after the NSSM test is compared in Fig. 7b. There is a very good correlation between these conductivities. However, it is observed that the conductivities after the NSSM test are 4–5% lower than those before the test. This is in contrast to the RCP test where the conductivities were 14–19% higher after the test. One reason could be the replacement of the Na^+ and OH^- ions having higher equivalent conductivities with Cl^- ions in the pore solution. This could also be due to microstructural changes that are induced by the NSSM process, which is the subject of a following section.

3.4. Pore structure and its effects on transport characteristics

The influence of the pore structure on the mechanical and durability properties of concretes is well-established. It is therefore important to evaluate the influence of pore structure features of alkali silicate powder activated concretes on the RCP and NSSM values in order to obtain a better understanding of the similarities and contrasts in the trends of these values. Mercury intrusion porosimetry (MIP) on 28-day moist cured paste specimens is used for pore structure characterization. The use of MIP as an indicator of the total pore volume is well-accepted, but its use for pore size determination is questioned [30,31] because of the presence of "pore-throats" in cement pastes. Mercury cannot intrude into some of the larger pores until the applied pressure is large enough

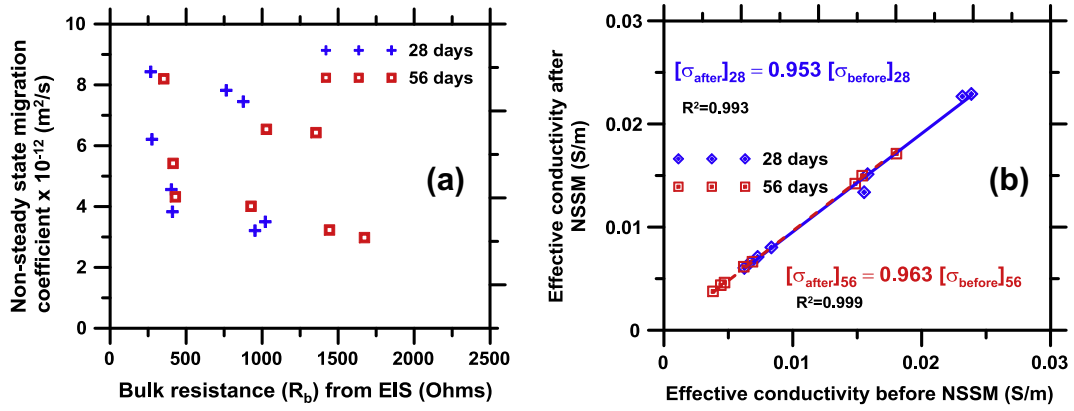

Fig. 7. Relationships between: (a) the bulk resistance (R_b) from EIS and the NSSM values, and (b) effective specimen conductivities before and after the NSSM test.

to saturate the pore throats. However, an indication of the threshold pore diameter, ideally not as an absolute value, but as a parameter to facilitate comparison between specimens, can be obtained from the differential pore volume-pore diameter relationships [32,33]. Fig. 8a and b depict the cumulative pore volume intruded by mercury and the differential pore volume ($dV/d\log D$) for the alkali silicate powder activated slag pastes proportioned using n values of 0.05 and 0.15 respectively and cured for 28 days. The cumulative pore volumes for all these cases are very similar (around 0.165 cm^3/g), showing that changing the n and M_s values within the range studied here does not influence the total pore volume in alkali silicate activated slag mixtures. However the RCP and NSSM values of the activated slag concretes are different for different activator parameters (n and M_s), necessitating the need to investigate the critical pore sizes.

The critical pore sizes or the threshold pore sizes are taken as the sizes corresponding to the maximum in the pore diameter (D) – $dV/d\log D$ relationships. It is the size below which the pore system is depercolated, and hence is crucial in determining the transport properties. A comparison of the threshold pore sizes (d_c) of the alkali silicate powder activated slag pastes shown in Fig. 8a and b indicate that they are different between mixtures made using different n and M_s values irrespective of the similarities in the overall pore volumes. Higher n value mixtures show markedly lower critical pore sizes. The total pore volume and critical pore size for a plain cement paste of similar water-to-cement ratio (w/c) are also shown in Fig. 8c, which are found to be comparable to that of the waterglass activated paste. When compared to those of the OPC and waterglass activated paste ($n = 0.05$, $M_s = 2.0$) shown in Fig. 8c, the critical pore sizes of alkali silicate powder activated pastes are much lower even though the total pore volume is higher for the powder activated pastes. The fundamental differences in the pore structure between the solid and liquid alkali silicate activated mixtures can be understood from Fig. 8. The total pore volume is more influential in determining the compressive strength of the material, as shown by the much higher strengths for the waterglass activated pastes depicted in Fig. 2 and elsewhere [16], whereas the critical pore size is more influential in the transport properties as observed from the higher RCP and NSSM values for the waterglass activated pastes as compared to the powder sodium silicate activated pastes [25]. A detailed treatment of this behavior and the proof for the dominance of pore sizes on the pore connectivity and thus the ionic transport properties in plain and modified concretes, based on electrical impedance spectroscopy and model analysis, have been provided in an earlier publication [27].

The critical pore sizes obtained from MIP are related to the parameter $n{\cdot}M_s$ in Fig. 9, as was shown for the RCP and NSSM values in Figs. 4 and 6, and a very similar relationship emerge. The critical pore sizes are found to decrease with increase in $n{\cdot}M_s$ (or the silica content in the activator), and beyond an $n{\cdot}M_s$ of about 0.10, the critical pore sizes are independent of $n{\cdot}M_s$. The same was found to be true for the RCP and NSSM values. This once again goes onto show that there is a limiting value of $n{\cdot}M_s$ beyond which further reaction product formation and refinement of the pore structure does not happen. This result therefore can be used in the material design of alkali silicate powder activated slag mixtures.

3.5. Microstructural modeling using electrical impedance circuits and associated parameters

3.5.1. Electrical circuit model and associated parameters

The Nyquist plots obtained from EIS contains several features of the material microstructure that are otherwise difficult to deter-

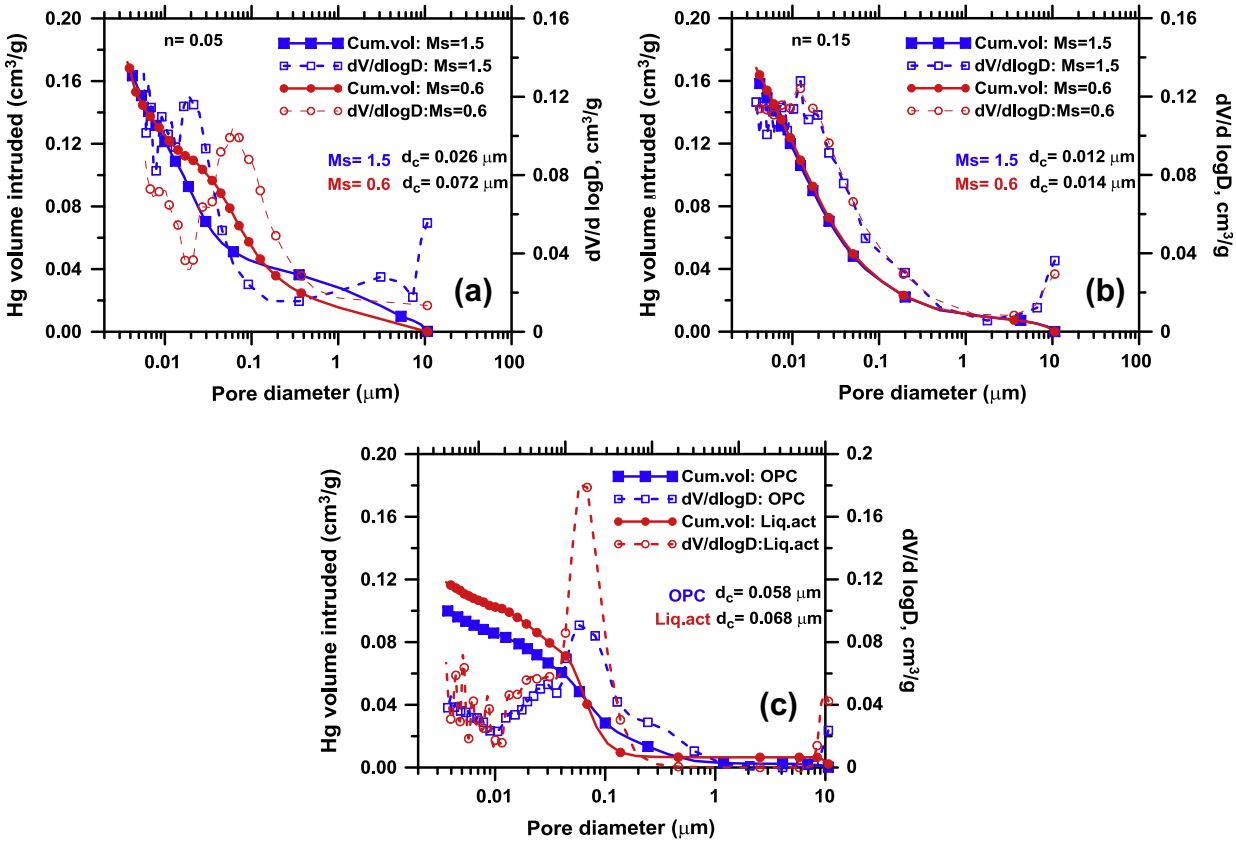

Fig. 8. MIP curves showing the cumulative pore volume intruded and the differential pore volume as a function of pore diameter for: (a) powder activated pastes; $n = 0.05$; (b) powder activated pastes; $n = 0.15$; and (c) OPC and liquid activated ($n = 0.05$, $M_s = 2.0$) pastes.

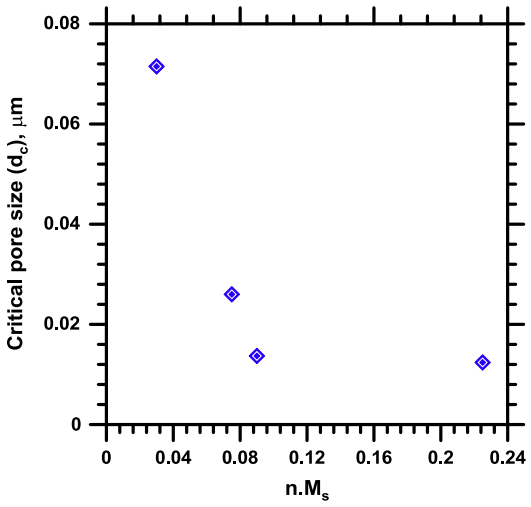

Fig. 9. Relationship between $n{\cdot}M_s$ and critical pore size from MIP.

mine. Different types of equivalent electrical circuit models have been used to represent the Nyquist plots of cement-based materials. Equivalent electrical circuits are a combination of resistors, capacitors, and/or constant-phase elements, which when assembled in certain configurations, provide reliable representations of the pore structure of the material. Among several equivalent electrical circuits used in the study of cement-based materials, the one depicted in Fig. 10a has been shown to adequately capture the material structure [27,34–36], and hence is used in this study. This model accounts for only the bulk arc in a typical Nyquist plot. The resistance R_e in the circuit denotes the resistance of electrolytes between the electrodes and the concrete sample in the NSSM test set up. The resistance R_c is associated with the connected pores in the concrete (percolating pores), while R_{uc} is the resistance of the unconnected or isolated pores in the material structure. C_1 is the dielectric capacitance related to the solid phase in the concrete (paste and the aggregates), and C_2 is the capacitance associated with the double layer present between the pore walls and the pore solution. R_i and C_3 denote the resistance and capacitance of the specimen-electrode interface. The total frequency dependent impedance $Z(\omega)$ of the system can be represented as:

$$Z(w) = R_e + \frac{Z_1 Z_2}{Z_1 + Z_2} + Z_3 \tag{4}$$

Z_1, Z_2, and Z_3 are the impedances of the element groups in the circuit. The impedances Z_1 and Z_2, belonging to the R_c–C_1 and R_{uc}–C_2 combinations respectively (bulk part of the system) are denoted as:

$$Z_1 = \frac{R_c}{1 + (j\omega R_c C_1)^{\alpha}} \tag{5a}$$

$$Z_2 = R_{uc}[1 + (j\omega R_{uc} C_2)^{-\beta}] \tag{5b}$$

The terms α and β are the dispersion factors. The equivalent circuit model parameters were extracted from the impedance spectra using ZView™ software. Fig. 10b shows the EIS spectra and representative fits obtained from the equivalent electrical circuit for the bulk arc for two selected activated slag concretes. It can be seen that the fits are in good agreement with the measured impedance spectra.

3.5.2. Inferring the changes in material microstructure through circuit model parameters

The variation in electrical circuit parameters as described above can also provide indications of the microstructural changes in concretes as a result of chloride ion transport. The resistance of the connected pores is one of the most important model parameters that relate to the microstructure because the transport is dominated by the connected (percolating) pores. This parameter relates very well to the bulk resistance (R_b) as shown in Fig. 11. It was shown in the earlier section that the conductivities after the RCP test were higher by about 14–19% and those after the NSSM test were lower by about 4–5% than the values before the test. Using the microstructural parameters derived from the circuit model, this section evaluates the reasons for the changes in the electrical properties before and after the RCP and NSSM tests.

Fig. 12a shows the relationship between resistances from the circuit model (R_c and R_{uc}, the resistances of the connected and unconnected pores respectively) before and after the RCP test. There is about a 5–10% decrease in both the R_c and R_{uc} values after the test, which corresponds well with the increase in conductivity after RCP test shown in Fig. 5b. Ideally, the unconnected pore resistance should remain unchanged because they do not participate in transport to a large extent. The change in the modeled pore resistances after the RCP test can be regarded as an indication of the damage in material microstructure imposed by the higher voltages and associated temperature increase during the RCP test as has been reported elsewhere [28]. Fig. 12b depicts the relationship between R_c and R_{uc} from the circuit model before and after the NSSM

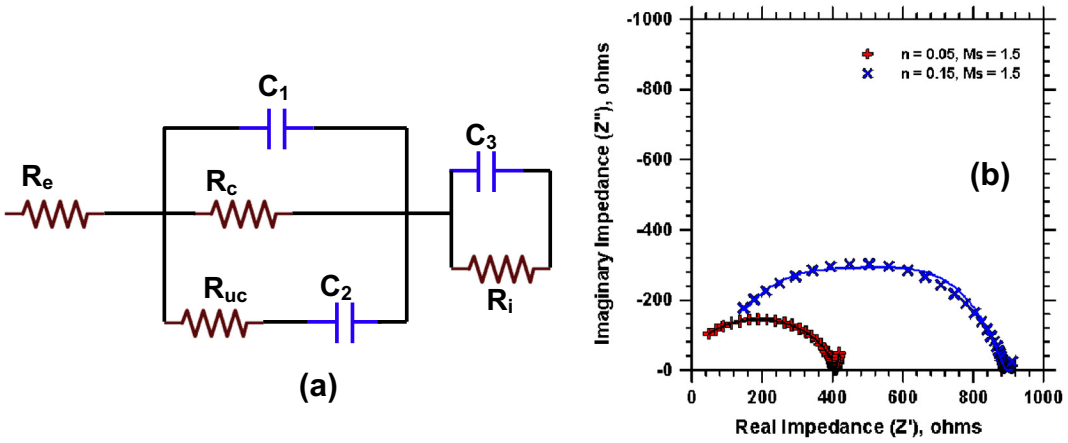

Fig. 10. (a) Equivalent circuit model for electrical impedance response, and (b) a fit of the model to typical Nyquist plots.

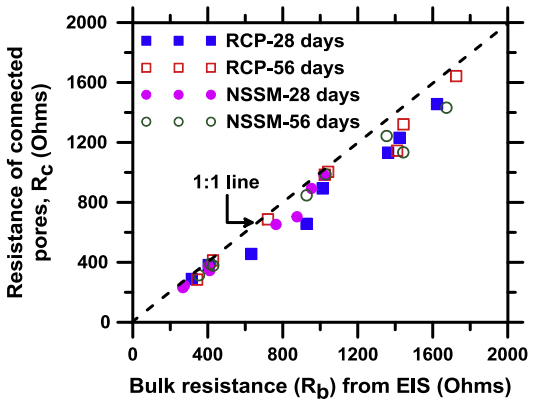

Fig. 11. Relationship between the bulk resistance and the resistance of the connected pores.

test. There is a small increase in the resistance of the connected pores (as opposed to the decrease in resistance observed after the RCP test), but the resistance of unconnected pores remain practically unchanged, in contrast to the observations for the RCP test. Since the unconnected pores do not participate in transport, this is expected. The increase in resistance of the connected pores may be an indication of the formation of new solid products aided by the ingress of chloride ions or the replacement of highly conductive OH^- ions by the less conductive Cl^- ions. However, in the non-steady state test time interval, it is less likely that the OH^- ions are removed from the specimen [37,38]. The increase in bulk resistances and the resistance of the connected pores after the NSSM test therefore could be construed as an indication of the formation of new solid products either within the pores or as electrochemical double layers along the pore walls [39]. Large changes in porosity are not expected, and it has been shown experimentally [40] that the porosity changes slightly only in the anolyte side during a NSSM test. Thus the microstructural parameter that changes as a result of non-steady state chloride migration is likely the pore connectivity factor (because effective conductivity, $\sigma_{eff} = \sigma_o \phi \beta$, where σ_o is the pore solution conductivity, ϕ is the porosity, and β is the pore connectivity factor [27]).

The relationships between the capacitance representing the solid phase in the concrete (C_1), and that associated with the double layer between the pore walls and the pore solution (C_2) before and after the transport tests shed more light on the changes induced by the accelerated chloride transport tests on the material microstructure of alkali silicate powder activated slag concretes. Fig. 13a and b show the relationships between the capacitances (C_1 and C_2) before and after the RCP and NSSM tests respectively. For the RCP test (Fig. 13a), the capacitance attributed to the solid phase (C_1) does not change at all because of the test, whereas for the NSSM test (Fig. 13b), there is a slight increase in C_1, which is similar in magnitude to the increase in R_c shown in Fig. 12b. This is an indication of slight changes in the solid phase microstructure due to the migration test; potentially a minimal reduction in porosity. However, when the pore wall-pore solution interfacial capacitance (C_2) is considered, there is a slight increase after the RCP test, but a much higher increase after the NSSM test as observed from comparisons between Fig. 13a and b. This likely denotes the formation

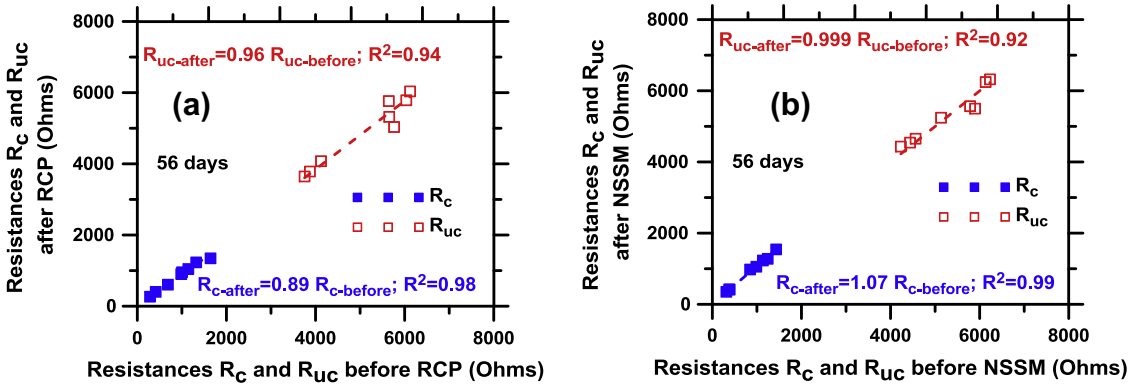

Fig. 12. Relationships between the resistances of the connected (R_c) and unconnected (R_{uc}) pores extracted from the circuit model before and after the: (a) RCP test, and (b) NSSM test.

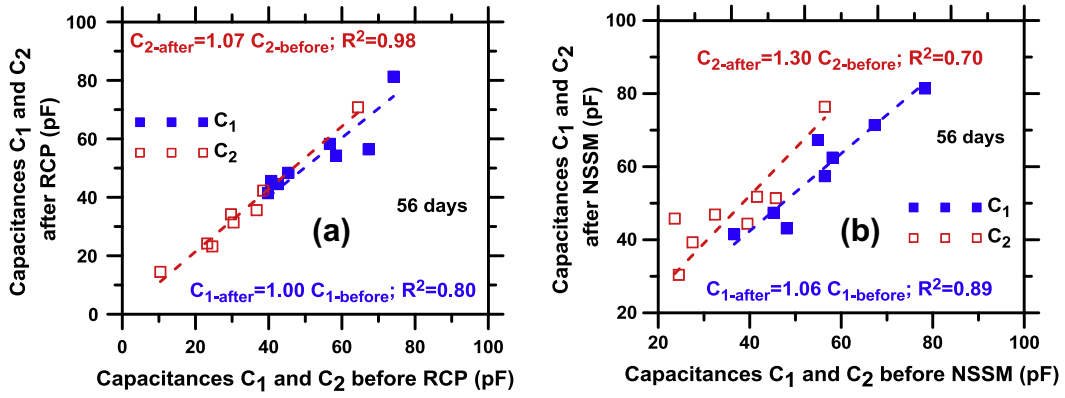

Fig. 13. Relationships between the capacitances of the solid phase (C_1) and pore wall-pore solution interface (C_2) extracted from the circuit model before and after the: (a) RCP test, and (b) NSSM test.

of reaction products along the pore walls as a result of binding of chloride ions in the longer duration NSSM test. The binding product formation along the pore walls increases the surface area of the pores [35,36], consequently influencing the transport lengths. Thus the pore tortuosity (which is proportional to the inverse of the square root of pore connectivity [27]) of the pore system in alkali activated concretes is impacted by the NSSM test, confirming the inference arrived at based on the changes in resistances in the previous paragraph. While the amount of bound chlorides in non-steady state migration and natural diffusion experiments have been reported to be similar in OPC concretes provided that the external chloride concentrations are high enough (>1 M) [41], the presence of higher alkalinity in the pore solution (which can be expected for alkali activated concretes) reduces the formation of chloride binding products in the C–S–H [42]. A quantification of chloride binding has not been attempted in this paper. A comparison with a recent study that dealt with EIS circuit modeling of OPC concretes subjected to NSSM tests [34] showed that the increase in interfacial capacitance after the NSSM test for the alkali activated concretes studied in this paper is only about 60% of that for OPC concretes. This substantiates the fact that a higher alkalinity reduces the binding of chloride ions in C–S–H gel.

4. Conclusions

This paper has presented a thorough investigation of chloride transport in alkali silicate powder activated slag concretes evaluated using accelerated test methods and electrical impedance spectroscopy. The influence of the pore structure on the transport properties and the changes in pore structure as a result of accelerated ionic transport has been brought out.

The RCP values of the alkali silicate powder activated slag concretes were found to be generally lower than those of OPC concretes or waterglass activated slag concretes, but their NSSM coefficients were similar to those of OPC and waterglass activated slag concretes. It could therefore be safely stated that sodium silicate powder activated slag concretes have comparable chloride transport resistance as that of OPC or waterglass activated slag concretes. It was observed that both the 28- and 56-day RCP and NSSM values decrease with increase in the activator parameter $n{\cdot}M_s$ (corresponding to the silica content in the activator), with a limiting value of 0.10 for $n{\cdot}M_s$ beyond which the chloride transport parameters are insensitive to the activator parameter. When the electrical conductivities of the specimens before and after the transport tests were compared, the RCP test was found to result in a higher specimen conductivity after the test, possibly contributed by the ingress of chloride ions and the damage in material microstructure as a result of higher voltages and associated temperature increase. The specimen conductivities were found to reduce slightly after the NSSM test, pointing to the potential formation of binding products.

While it was observed that the cumulative pore volumes intruded by mercury are similar for the alkali silicate powder activated slag pastes irrespective $n{\cdot}M_s$, the critical pore sizes (d_c) were found to be very different. The relationship between $n{\cdot}M_s$ and d_c was found to be similar to the relationships between $n{\cdot}M_s$ and RCP or NSSM values. It was also shown that the critical pore size is more influential than porosity in determining the chloride transport properties of concretes.

The resistances and capacitances extracted from the fits of the circuit models to the Nyquist plot revealed important features of the pore structure as related to accelerated chloride transport. The resistance of the connected pores (R_c) obtained from the circuit model was found to be very similar to the bulk resistance of the specimens (R_b). R_c decreases after the RCP test whereas it increases after the NSSM test. This might be considered as an indication of microstructural damage after the RCP test, and the formation of additional chloride binding products after the NSSM test. Capacitances derived from the circuit models provided more details on this response. While the pore wall-pore solution interfacial capacitance showed only a marginal change for the specimens after the RCP test, a much higher increase was noticed after the NSSM test, denoting the microstructural changes along the pore walls. The pore tortuosity and the transport lengths were found to be influenced much more than the porosity (as observed from negligible changes in the solid phase capacitance C_1) by the NSSM test. EIS combined with electrical circuit modeling was shown to be efficient non-invasive strategy to understand the influence of accelerated test methods on the material microstructure.

Acknowledgements

The authors sincerely acknowledge the funding from New York State Energy Research and Development Authority (NYSERDA) towards the conduct of this study. The materials were supplied by Holcim US and PQ Corporation, which is gratefully acknowledged. The experimental work was carried out in the Laboratory for the Science of Sustainable Infrastructural Materials (LS-SIM) at Arizona State University (ASU). The contents of this paper reflect the views of the authors who are responsible for the facts and accuracy of the data presented herein, and do not necessarily reflect the views and policies of the funding agency, nor do the contents constitute a standard, specification, or a regulation.

References

[1] Roy DM, Jiang W, Silsbee MR. Chloride diffusion in ordinary, blended, and alkali-activated cement pastes and its relation to other properties. Cem Concr Res 2000;30(12):1879–84.
[2] Shi C, Krivenko PV, Roy D. Alkali-activated cements and concretes. Spon Press; 2006.
[3] Palomo A, Grutzeck M, Blanco M. Alkali-activated fly ashes: a cement for the future. Cem Concr Res 1999;29(8):1323–9.
[4] Altan E, Erdoğan ST. Alkali activation of a slag at ambient and elevated temperatures. Cem Concr Compos 2012;34(2):131–9.
[5] Haha MB, Lothenbach B, Le Saout G, Winnefeld F. Influence of slag chemistry on the hydration of alkali-activated blast-furnace slag—Part II: Effect of Al_2O_3. Cem Concr Res 2012;42(1):74–83.
[6] Haha MB, Lothenbach B, Le Saout G, Winnefeld F. Influence of slag chemistry on the hydration of alkali-activated blast-furnace slag—Part I: Effect of MgO. Cem Concr Res 2011;41(9):955–63.
[7] Brough AR, Atkinson A. Sodium silicate-based, alkali-activated slag mortars: Part I. Strength, hydration and microstructure. Cem Concr Res 2002;32(6):865–79.
[8] Bakharev T, Sanjayan JG, Cheng Y. Alkali activation of Australian slag cements. Cem Concr Res 1999;29(1):113–20.
[9] Fernández-Jiménez A, Palomo JG, Puertas F. Alkali-activated slag mortars: mechanical strength behaviour. Cem Concr Res 1999;29(8):1313–21.
[10] Aydın S, Baradan B. Mechanical and microstructural properties of heat cured alkali-activated slag mortars. Mater Des 2012;35:374–83.
[11] El-Didamony H, Amer AA, Abd Ela-ziz H. Properties and durability of alkali-activated slag pastes immersed in sea water. Ceram Int 2012;38(5):3773–80.
[12] Duran Atiş C, Bilim C, Çelik Ö, Karahan O. Influence of activator on the strength and drying shrinkage of alkali-activated slag mortar. Constr Build Mater 2009;23(1):548–55.
[13] Sakulich AR, Anderson E, Schauer C, Barsoum MW. Mechanical and microstructural characterization of an alkali-activated slag/limestone fine aggregate concrete. Constr Build Mater 2009;23(8):2951–7.
[14] Yang K, Song J, Ashour AF, Lee E. Properties of cementless mortars activated by sodium silicate. Constr Build Mater 2008;22(9):1981–9.
[15] Fernández-Jiménez A, Puertas F. Alkali-activated slag cements: kinetic studies. Cem Concr Res 1997;27(3):359–68.
[16] Ravikumar D, Neithalath N. Reaction kinetics in sodium silicate powder and liquid activated slag binders evaluated using isothermal calorimetry. Thermochim Acta 2012;546:32–43.
[17] Ravikumar D, Neithalath N. Effects of activator characteristics on the reaction product formation in slag binders activated using alkali silicate powder and NaOH. Cem Concr Compos 2012;34(7):809–18.
[18] Shi C. Strength, pore structure and permeability of alkali-activated slag mortars. Cem Concr Res 1996;26(12):1789–99.

[19] Lecomte I, Henrist C, Liégeois M, Maseri F, Rulmont A, Cloots R. (Micro)-structural comparison between geopolymers, alkali-activated slag cement and Portland cement. J Eur Ceram Soc 2006;26(16):3789–97.
[20] Bernal SA, Mejía de Gutiérrez R, Pedraza AL, Provis JL, Rodriguez ED, Delvasto S. Effect of binder content on the performance of alkali-activated slag concretes. Cem Concr Res 2011;41(1):1–8.
[21] Bernal SA, Mejía de Gutiérrez R, Provis JL. Engineering and durability properties of concretes based on alkali-activated granulated blast furnace slag/metakaolin blends. Constr Build Mater 2012;33:99–108.
[22] Neithalath N. Extracting the performance predictors of enhanced porosity concretes from electrical conductivity spectra. Cem Concr Res 2007;37(5):796–804.
[23] Cook RA, Hover KC. Mercury porosimetry of hardened cement pastes. Cem Concr Res 1999;29(6):933–43.
[24] Abell AB, Willis KL, Lange DA. Mercury intrusion porosimetry and image analysis of cement-based materials. J Colloid Interface Sci 1999;211(1):39–44.
[25] Ravikumar D, Neithalath N. Electrically induced chloride ion transport in alkali activated slag concretes and the influence of microstructure. Cem Concr Res 2013;47:31–42.
[26] Spiesz P, Brouwers HJH. Influence of the applied voltage on the Rapid Chloride Migration (RCM) test. Cem Concr Res 2012;42(8):1072–82.
[27] Neithalath N, Jain J. Relating rapid chloride transport parameters of concretes to microstructural features extracted from electrical impedance. Cem Concr Res 2010;40(7):1041–51.
[28] Julio-Betancourt GA, Hooton RD. Study of the Joule effect on rapid chloride permeability values and evaluation of related electrical properties of concretes. Cem Concr Res 2004;34(6):1007–15.
[29] Neithalath N, Persun JD, Manchiryal R. Electrical conductivity based microstructure and strength prediction of plain and modified concretes. Int J Adv Eng Sci Appl Math 2010;2:83–94.
[30] Diamond S. Mercury porosimetry: an inappropriate method for the measurement of pore size distributions in cement-based materials. Cem Concr Res 2000;30(10):1517–25.
[31] Moro F, Böhni H. Ink-bottle effect in mercury intrusion porosimetry of cement-based materials. J Colloid Interface Sci 2002;246(1):135–49.
[32] Atahan HN, Oktar ON, Taşdemir MA. Effects of water–cement ratio and curing time on the critical pore width of hardened cement paste. Constr Build Mater 2009;23(3):1196–200.
[33] Ye G, Liu X, De Schutter G, Poppe AM, Taerwe L. Influence of limestone powder used as filler in SCC on hydration and microstructure of cement pastes. Cem Concr Compos 2007;29(2):94–102.
[34] Jain J, Neithalath N. Electrical impedance analysis based quantification of microstructural changes in concretes due to non-steady state chloride migration. Mater Chem Phys 2011;129(1–2):569–79.
[35] Sánchez I, Nóvoa XR, de Vera G, Climent MA. Microstructural modifications in Portland cement concrete due to forced ionic migration tests. Study by impedance spectroscopy. Cem Concr Res 2008;38(7):1015–25.
[36] Díaz B, Nóvoa XR, Pérez MC. Study of the chloride diffusion in mortar: a new method of determining diffusion coefficients based on impedance measurements. Cem Concr Compos 2006;28(3):237–45.
[37] Zhang T, Gjørv OE. An electrochemical method for accelerated testing of chloride diffusivity in concrete. Cem Concr Res 1994;24(8):1534–48.
[38] Yang CC, Cho SW, Chi JM, Huang R. An electrochemical method for accelerated chloride migration test in cement-based materials. Mater Chem Phys 2003;77(2):461–9.
[39] Siegwart M, Lyness JF, McFarland BJ. Change of pore size in concrete due to electrochemical chloride extraction and possible implications for the migration of ions. Cem Concr Res 2003;33(8):1211–21.
[40] Díaz B, Freire L, Merino P, Nóvoa XR, Pérez MC. Impedance spectroscopy study of saturated mortar samples. Electrochim Acta 2008;53(25):7549–55.
[41] Castellote M, Andrade C, Alonso C. Chloride-binding isotherms in concrete submitted to non-steady-state migration experiments. Cem Concr Res 1999;29(11):1799–806.
[42] Nielsen EP, Herfort D, Geiker MR. Binding of chloride and alkalis in Portland cement systems. Cem Concr Res 2005;35(1):117–23.